AGU
ADVANCING
EARTH AND
SPACE SCIENCE

JGR Space Physics

Key Points:
- Nighttime medium-scale traveling ionospheric disturbances (MSTIDs) occur less frequently over northern Germany than at lower latitude regions
- The presence of Es layers with sporadic-E trace is observed greater than 4 MHz is a potential source for the onset of the observed MSTIDs
- The low occurrence rate and small amplitude of nighttime MSTIDs could be attributed to the dip angle dependence of the Es layer instability

Supporting Information:
Supporting Information may be found in the online version of this article.

Correspondence to:
M. Sivakandan,
mani@iap-kborn.de;
skandanm89@gmail.com

On the Role of E-F Region Coupling in the Generation of Nighttime MSTIDs During Summer and Equinox: Case Studies Over Northern Germany

Mani Sivakandan[1] [ID], **Carlos Martinis[2]** [ID], **Yuichi Otsuka[3]** [ID], **Jorge L. Chau[1]** [ID], **Jessica Norrell[2]**, **Jens Mielich[1]** [ID], **J. Federico Conte[1]** [ID], **Claudia Stolle[1]** [ID], **J. Rodríguez-Zuluaga[4]** [ID], **Atsuki Shinbori[3]** [ID], **Michi Nishioka[5]** [ID], and **Takuya Tsugawa[5]**

[1]Leibniz Institute of Atmospheric Physics at the University of Rostock (IAP), Kühlungsborn, Germany, [2]Center for Space Physics, Boston University, Boston, MA, USA, [3]Institute for Space Earth Environmental Research (ISEE), Nagoya University, Nagoya, Japan, [4]GFZ German Research Centre for Geosciences, Potsdam, Germany, [5]National Institute of Information and Communications Technology, Tokyo, Japan

Abstract Simultaneous observations from a 630 nm all-sky airglow imager, GNSS-TEC receivers, and an ionosonde are used to investigate the role of E- and F-region coupling on the generation of medium-scale traveling ionospheric disturbances (MSTIDs). The primary observations are OI 630 nm airglow images taken by an all-sky imager in Kühlungsborn (54.07°N; 11.46°E, 53.79°N Mlat.), a site in northern Germany. Out of 226 nights of observations, MSTIDs were found only in 18 nights, demonstrating the low occurrence rate over Kühlungsborn. We focused on four MSTIDs events: two during the vernal equinox and two during summer. Coincident measurements of detrended GNSS-TEC supported the presence of MSTIDs during the selected events, and simultaneous observations from the ionosonde in Juliusruh (54.60°N, 13.4°E, 54.02°N Mlat.) showed sporadic-E (Es) layer and spread-F activity in the E- and F-region, respectively. We observed the onset of the observed MSTIDs to be around the 15°–20°E longitude and 60–45°N latitude belts. Additionally, we found that in each case, the onset of MSTIDs coincides with the presence of an Es layer with sporadic-E trace is observed (foEs) exceeding 4 MHz. This suggests that an Es layer with foEs $\geq$ 4MHz was a source of the generation of these MSTIDs. Altitude of the Es layer could be another important factor in generating MSTIDs. The Es layer should exist at an altitude where Hall conductivity is large, as happened in the present study.

1. Introduction

Nighttime ionospheric structures, with phase fronts oriented northwest to southeast and propagating southwestward, are commonly observed at mid-latitudes in the northern hemisphere during solstice months (Kotake et al., 2007; Martinis et al., 2010; Shiokawa, Ihara, et al., 2003; Shiokawa, Otsuka, et al., 2003). These features are identified as nighttime medium-scale traveling ionospheric disturbances (MSTIDs). Initially considered a manifestation of neutral atmospheric gravity waves (Bowman, 1990; Bowman & Monro, 1988), later investigations showed an association between MSTIDs and electric field perturbations (Behnke, 1979; Shiokawa, Ihara, et al., 2003; Shiokawa, Otsuka, et al., 2003) and mostly confined these features to the middle and low latitude ionosphere (Narayanan et al., 2014; Shiokawa, Ihara, et al., 2003; Shiokawa, Otsuka, et al., 2003). Furthermore, the electrical nature of nighttime MSTIDs is supported by observations of geomagnetic conjugacy (Martinis et al., 2011, 2019; Otsuka et al., 2004; Shiokawa et al., 2005). Studies have also suggested that MSTID activity, measured as TEC perturbations, is correlated with sporadic E (Es) layer activity (Otsuka et al., 2008).

The cause of nighttime MSTIDs was once attributed to be the Perkins instability mechanism (Perkins, 1973), but further developments showed that the growth rate of the instability is too small to explain the observed perturbations (Shiokawa, Ihara, et al., 2003; Shiokawa, Otsuka, et al., 2003; Tsunoda & Cosgrove, 2001). More recently, model simulations and observational studies have suggested MSTID generation is caused by coupling between the F-region and E-region instabilities, such as quasi-periodic echoes, unstable Es layers, and Es layer instability (Cosgrove et al., 2004; Haldoupis et al., 2003; Yokoyama et al., 2009). For example, Saito et al. (2007) showed a good correlation between the occurrence of quasi-periodic echoes in the E-region and MSTIDs in the F-region by using the middle and upper atmosphere (MU) radar and GNSS-TEC observations. Nevertheless, they could not provide conclusive evidence about which region acted as a source for the other. A study by Haldoupis et al. (2003) proposed that an enhanced polarization electric field inside unstable Es layer patches can

contribute to the formation of mid-latitude spread-F through magnetic field line mapping. Furthermore, Cosgrove et al. (2004) derived a linear growth rate for the coupled system of the Es layer and F-region by realizing the unified formalism for the Es layers and Perkins instabilities. When calculating the coupled Es layer and F-region instabilities, they noted a significant enhancement in the growth rate. Cosgrove (2013) then used a model simulation to argue that the ratio of the field line integrated Hall conductivity ($\sum$H) of the Es layer to the field line integrated Pedersen conductivity ($\sum$PF) of the F-region has an important role in controlling the influence of the E-region polarization electric field on the F-region. He also showed that when the conductance ratio is unity, the Es layer polarization electric field exerts a significant effect on the F-layer.

In addition to local factors, the source of nighttime MSTIDs observed in one hemisphere may originate in the opposite hemisphere, a result indicative of their geomagnetic conjugate nature. This concept was examined in Yokoyama (2014), where the simultaneous occurrence of nighttime MSTIDs at magnetic conjugate locations was reproduced in a simulation when two conditions were met. First, the F-region neutral wind needed to satisfy an unstable condition in both hemispheres, and second, a sporadic-E layer had to be present in at least one hemisphere. Observations of geomagnetic conjugacy were presented in Narayanan et al. (2018), relying on simultaneous E- and F-region measurements from the geomagnetic conjugate points over two geomagnetically conjugate points: Sata, Japan and Darwin, Australia. This study examined the onset of MSTIDs as well as F-region inter-hemispheric coupling processes and found that simultaneous MSTIDs occurred when there was strong Es layer activity in at least one hemisphere. They defined strong Es layer activity as sporadic-E trace is observed (foEs) greater than 6 MHz and the difference between sporadic-E trace is observed (foEs) and F-layer is blanked out (fbEs) greater than 5 MHz. These results were consistent with simulations by Yokoyama (2014), as detailed previously. Going further, Narayanan et al. (2018) showed that MSTIDs can appear simultaneously in both hemispheres even with unfavorable thermospheric winds in one. This finding in particular did not agree with results of hemisphere-coupled models.

Another important aspect of nighttime MSTIDs is their seasonal and longitudinal variation over mid-latitudes. In the Japanese sector, 630 nm airglow and GNSS-TEC observations showed an occurrence rate of MSTIDs with two distinct peaks: a primary peak in summer and secondary peak in winter (Otsuka et al., 2021; Shiokawa, Ihara, et al., 2003; Shiokawa, Otsuka, et al., 2003). A similar pattern was reported over North America and Europe, with the maxima of MSTIDs occurrences coinciding with solstices and the minima with equinoxes (Martinis et al., 2010; Otsuka et al., 2013; Terra et al., 2020). Martinis et al. (2010) suggested Es layers and interhemispheric coupling as a possible generation mechanism of nighttime MSTIDs, thereby explaining the observed semiannual variation. This further supported the notion that the longitudinal variation of the occurrence of Es layers can plausibly be a reason for the longitudinal variation of occurrence of MSTIDs (Otsuka et al., 2008).

It has also been shown that the solar cycle plays a part in the occurrence of MSTIDs, with a higher rate during solar minimum than maximum. Studies argued that the growth rate of the Perkins instability is inversely proportional to the ion-neutral collision frequency, and that this could be a reason for the solar cycle dependency of nighttime MSTIDs (Duly et al., 2013; Martinis et al., 2010; Otsuka et al., 2021). A different study by Terra et al. (2020) reported that nighttime MSTIDs show a positive (June solstice) and negative (December solstice) correlation with solar activity and that the changes in the wind direction during the summer and winter solstices could cause the asymmetry in the solar cycle dependence of the nighttime MSTIDs in different seasons.

Other investigations showed that equatorward propagation of the nighttime MSTIDs can be impeded by the presence and strength of the equatorial ionization anomaly (EIA), (Narayanan et al., 2014; Shiokawa et al., 2002; Sivakandan et al., 2019). If there is a weak (EIA) or none at all, nighttime MSTIDs can ingress into very low geomagnetic latitudes (Sivakandan et al., 2019). Upon reaching these geomagnetic low and equatorial latitudes, MSTIDs can act as a seed perturbation for midnight equatorial plasma bubbles/irregularities (Takahashi et al., 2018) and could themselves cause the meter-scale irregularities and spread-F in the low latitude ionosphere (Narayanan et al., 2019). Many studies aim to understand the low latitude limit for the onset of MSTIDs, but studies focusing on high latitude limit for the occurrence of southwest moving nighttime MSTIDs are limited.

One of the few high latitude studies was by Otsuka et al. (2013) and used 2-dimensional TEC maps to observe the latitudinal and longitudinal variation of nighttime MSTIDs over Europe during the low solar activity year of 2008. They observed that the occurrence rate of MSTIDs was higher at latitudes below 55°N rather than above. Furthermore, the occurrence rate below 55°N is higher during the winter solstice than during the summer

solstice. Shiokawa et al. (2013) investigated MSTIDs occurrences over Tromsø, a high latitude station in Norway, between January 2009 and March 2010. The results showed that the occurrence rate is higher in pre-midnight hours. Most cases had either eastward or westward propagation, but some few had southwestward propagation. They suggested that Perkins-associated E-F coupling instabilities and gravity waves from the lower atmosphere as the primary and secondary sources, respectively, of the observed MSTIDs. Neither this study, nor the one carried out in Otsuka et al. (2013) used concurrent observations from the E-region.

This study aims to use simultaneous observations of the E- and F-region made by multiple instruments both to investigate the role of E- and F-region coupling processes on the generation of nighttime MSTIDs over a mid-latitude transition region in Europe and to test a high latitude limit for the onset of nighttime MSTIDs. Observations are focused on the all-sky airglow imager in Kühlungsborn, Germany and involve four dates: 14 March 2020; 23 March 2020; 28 August 2017, and 28 May 2020. These observations are complemented by detrended GNSS-TEC measurements, and observations from the ionosonde in Juliusruh.

Data and analysis methodology, observations, and discussion are provided in Sections 2, 3, and 4, respectively, and the summary and conclusion are given in Section 5.

2. Data and Analysis Methodology

2.1. Airglow Imaging Observation

A Boston University all-sky imager (ASI) was installed in December 2016 at the Leibniz Institute of Atmospheric Physics (IAP) in Kühlungsborn (54.07°N; 11.46°E, 53.79°N magnetic latitude), a high mid-latitude transition region over northern Germany. The Institute of Atmospheric Physics (IAP) all-sky imager system, part of the network of all-sky imagers operated by Boston University (Martinis et al., 2018), is equipped with six interference filters enabling the observation of specific regions and processes. The present study utilized two filters: one enabling the observation of the thermospheric OI 630 nm redline emission (peak emission altitude at 250 km), and the other used for background measurement at a wavelength of 605.0 nm. The remaining four filters (three narrow bands and a wide band) are used to observe nightglow emissions in the mesosphere and lower thermosphere at wavelengths of 557.7 nm (green line), 589.3 (sodium emission), 864.5 nm (O_2 emission), and 695.0–1,050.0 nm (OH emission).

2.2. Ionosonde

The Institute of Atmospheric Physics (IAP) ionosonde at Juliusruh (54.60°N 13.40°E) is part of the international ionosonde network Global Ionospheric Radio Observatory (GIRO) (Reinisch & Galkin, 2011). Recently, Juliusruh data has been part of the TechTIDE project (Belehaki et al., 2020) and has been funded by the European Union's Horizon 2020 research and innovation program.

The ionosonde at Juliusruh is a Digisonde model DPS-4D and consists of two crossed rhombus antennae for transmission and four crossed loop antennae for reception (Reinisch et al., 2008). It swipes the ionosphere within a frequency range of 1–15 MHz and has one of the longest ionospheric time series with more than 60 years of continuous high-quality measurements.

Ionograms for the studied four nights were manually scaled. A sample ionogram with ionospheric characteristics is shown in Figure S1 of the Supporting Information S1. Characteristics for the Es background statistics were extracted from automatically scaled ionograms.

2.3. GNSS-TEC

The TEC maps were derived from GNSS observation data in Receiver INdependent EXchange format and obtained from the regional GNSS receiver network over Europe. Maps are provided through https://stdb2.isee.nagoya-u.ac.jp/GPS/GPS-TEC/ and a list of GNSS data providers can be found at https://stdb2.isee.nagoya-u.ac.jp/GPS/GPS-TEC/gnss_provider_list.html.
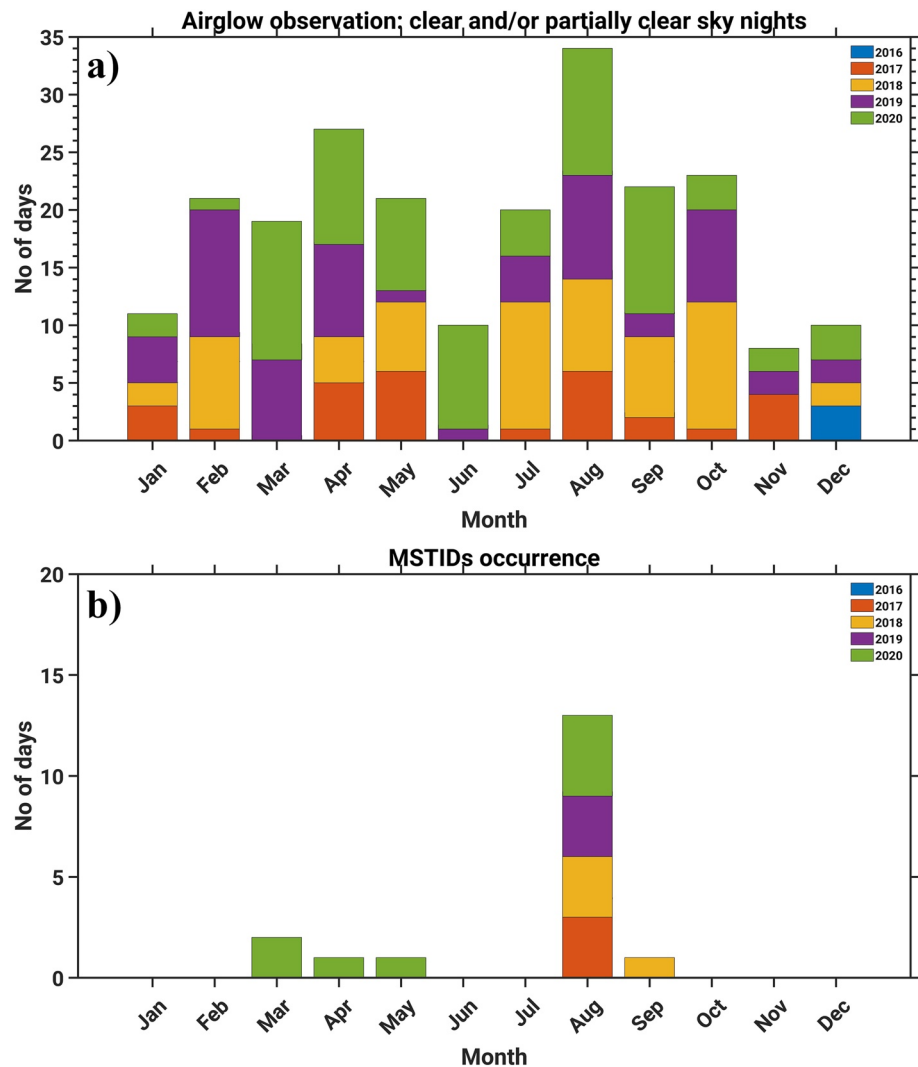
Figure 1. Airglow data availability with minimum 3 hr clear/partially clear sky nights from December 2016 to December 2020 sorted by month. Occurrence rate of nighttime medium-scale traveling ionospheric disturbances (MSTIDs) per month is shown in Figure 1b.

We estimated detrended TEC (dTEC) by subtracting 1-hr running averages from the original TEC for each pair of satellites and receivers (Otsuka et al., 2013). This allowed for the investigation of TEC variations caused by MSTIDs, as seen from GNSS data.

3. Observations

3.1. MSTIDs During Equinox and Summer Over Northern Germany

The onset of nighttime MSTIDs can be observed using 630.0 nm airglow imager data from Kühlungsborn (53.79°N Mlat.). Although observations are available as far back as late 2016, visibility can be limited by unfavorable conditions such as moonlight, or clouds, fog, etc. As a result, 226 nights are considered clear, or having more than 3 hr of cloudless conditions in a night, from the period between 2016 and 2020. From this data set, we observed only southwestward moving bright/dark bands—thought to be MSTIDs caused by the Perkins instability mechanism—in only 18. Out of these 18, thirteen nights are in August, three are in March, April and September each have one. All events had an onset after sunset and before midnight. Month wise data availability and the occurrences of MSTIDs are shown in Figures 1a and 1b, respectively. These results show the occurrence rate of

Table 1
MSTIDs Characteristics Deduced From OI 630 nm Airglow Emission Images Over Kühlungsborn, Germany

Sl.no	Date	Wavelength (km)	Phase speed (m/s)	Period (min)	Propagation direction
1	14.03.2020	397 ± 36	95 ± 9	69 ± 0.3	Southwest
2	23.03.2020	383 ± 23	127 ± 22	51 ± 6	Southwest
3	28.08.2017	340 ± 18	63 ± 6	90 ± 4	Southwest
4	28.05.2020	415 ± 28	145 ± 39	49 ± 10	Southwest

nighttime MSTIDs is not frequent over northern Germany and that the maximum occurrence rate is observed during the end of summer (i.e., August).

In the present analysis, we detail four events: two during summer solstice (28 August 2017 and 28 May 2020), and two during the vernal equinox (14 and 23 March 2020). These events were initially identified through airglow images.

To further enhance the visual contrast of airglow depletions in the chosen images, we first calculated the percentage difference image/residual image (Ip). Residual images are created by picking a central image (I) and averaging it with other images taken 30 min before and after. The resulting average (Ira) is therefore an hourly running average centered on I. From there, the hourly average is subtracted from and normalized with the central image to obtain the residuals ($Ip = (I - Ira)/Ira \times 100$). This method is widely used by the ionospheric community for the study of MSTIDs (Narayanan et al., 2014; Otsuka et al., 2004; Shiokawa, Ihara, et al., 2003; Shiokawa, Otsuka, et al., 2003; Sivakandan et al., 2019). These difference/residual images were then unwarped and projected onto an equidistant grid by assuming a 630 nm peak emission altitude centered at 250 km.

The MSTID parameters were derived from image analyses. When examining an image, the distance between peaks (maxima/minima) of two-phase fronts along the phase propagation direction is considered the wavelength. The temporal evolution of the positions of these phase fronts from a given image to the successive image provides phase velocity. Thus, the period of the MSTIDs is calculable using the horizontal wavelength and horizontal phase velocity. The derived MSTIDs parameters for each of the four nights in this study are given in Table 1, all of which are consistent with findings from past investigations. Details of the observed MSTIDs events are given below.

3.1.1. Event 1: 14 March 2020

Airglow observations began at 18:31 UT, or 19:31 Local Time (LT). A few sample percentage images for every half hour are shown in Figures 2a–2j. High airglow intensity regions are colored red in this figure, and low airglow intensity regions are blue. At around 20:03 UT, a dark phase front structure is seen between 55 and 50°N and 0°–20°E, aligned northwest to southeast. The structure propagates southwestwards with a horizontal phase velocity of 95 ± 9 m/s. The estimated horizontal wavelength and period of the MSTIDs are 397 ± 36 km and 69 ± 0.3 min, respectively. The amplitude of the MSTIDs ranged from −4 to 3%, where the perturbation is measured as a percentage. These amplitudes are smaller than those of typical mid-latitude MSTIDs which tend to be ∼10%–20% (Lee et al., 2008).

The phase fronts and amplitude of the MSTIDs were faint until 21:30 UT, at which point the amplitude gradually increased until several fronts can be seen at the center of the field of view (see the Movie S1 in the Supporting Information). The event was observable in the airglow images until 23:34 UT.

3.1.2. Event 2: 23 March 2020

Observations started at 18:50 UT, or 19:50 LT. Some percentage images for this night are shown in Figures 2k–2t. Structures aligned from the northwest to southeast appeared around 21:20 UT and spanned the region between 55 and 45°N and 10°–20°E (see the Movie S2). The structure in the image is colored blue to represent low airglow intensity, just as with Event 1. These blue band regions intensified over time and were followed by two additional blue bands.

One point to note is that there is a thin stretch of clouds alongside the blue northwest to southeast band in the images (see Figures 2k–2o) from 19:20 to 21:00 UT. The presence of clouds was confirmed via the visual inspection of raw 630.0 nm images and background 605.0 nm images.

The horizontal wavelength, phase velocity, and period of this MSTID were 383 ± 23 km, 127 ± 22 m/s, and 51 ± 6 min, respectively. Just as with Event 1, the amplitude of Event 2 ranges from −4 to 3%.
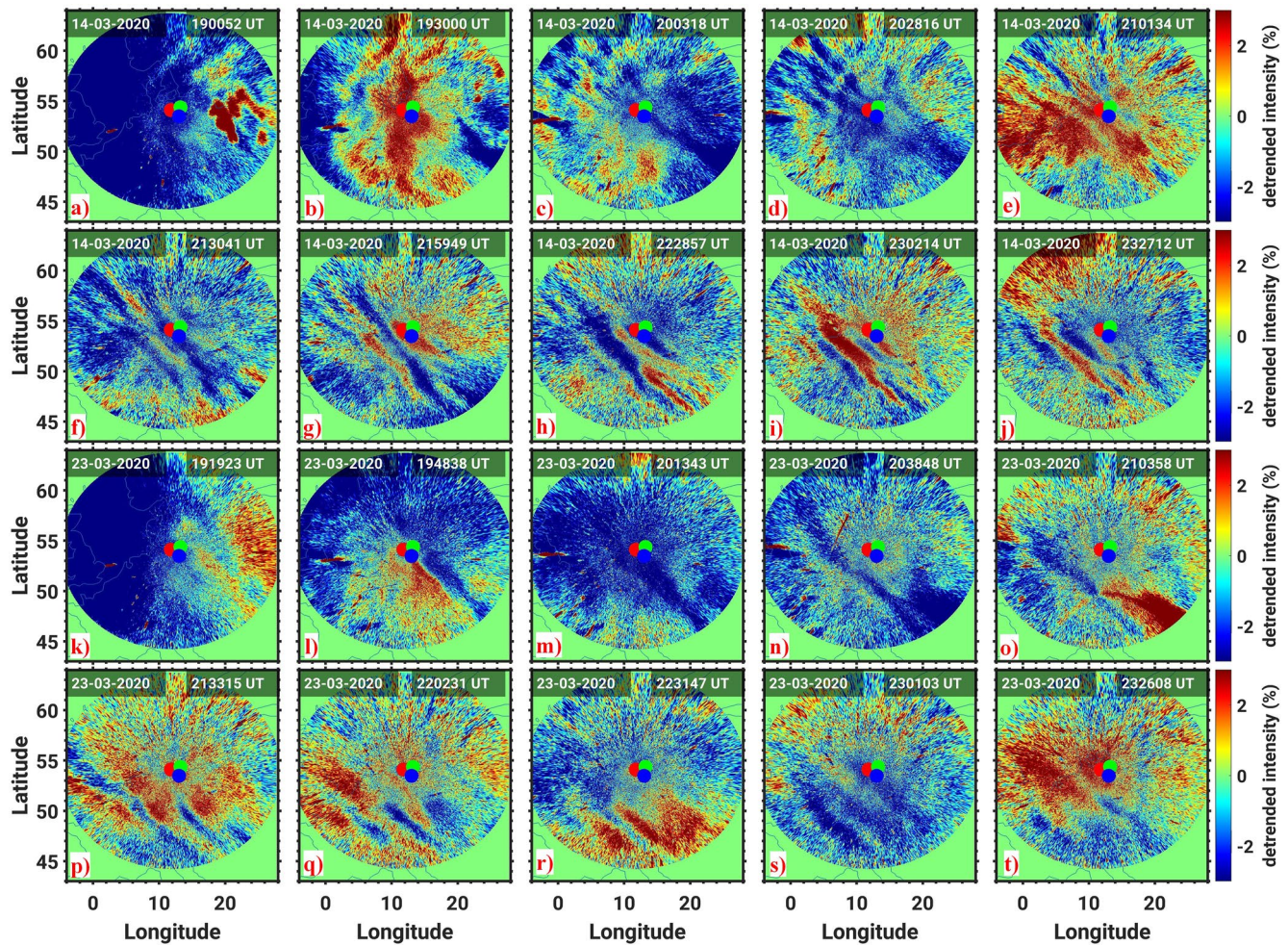
Figure 2. Residual 630 nm airglow images during equinox. The date and time are given in the top left and right corners of each image, respectively. Figures 2a–2j and 2k–2t show the presence of a phase front aligned from the northwest to the southeast. For both 14 and 23 March 2020 (Events 1 and 2), the phase front propagates toward the southwest. The location of the airglow imager at Kühlungsborn and ionosonde at Juliusruh are represented by red and green dots, respectively. The blue dot is the location of the E-region (∼100 km) when mapped into the F-region (250 km).

3.1.3. Event 3: 28 August 2017

Unlike the other events detailed in this study, the bands of Event 3 formed around 200–300 km northeast of Kühlungsborn. Figures 3a–3j show a few sample images for this event. The observations began at 19:41 UT, or 21:41 LT. Two faint blue bands were already visible at this time. One band was observed in the southwest, closer to the zenith, while the other was in the northeast, specifically the region between 50 and 60°N and 8°–18°E. Both propagated toward the southwest. An additional blue band was observed over Kühlungsborn around 21:00 UT (see Figure 3c), and was followed by several other blue bands, as seen in the successive images (see Movie S3). The MSTIDs were present in the field of view until 22:30 UT. The horizontal wavelength, phase velocity, and period of this MSTID were 340 ± 18 km, 63 ± 6 m/s, and 90 ± 4 min, respectively.

The event ended with faint northeastward propagating wave-like features above 55°N (see Figures 3h–3j).

3.1.4. Event 4: 28 May 2020

The structures were first observed over Kühlungsborn at 21:40 UT, or 23:40 LT. This image was the first taken on this evening of observations this is because earlier images would be too saturated by the moon's brightness. They were oriented from the northeast to the southwest and propagate southwestward (see Movie S4) with a horizontal phase velocity of 145 ± 39 m/s. The horizontal wavelength and period of the MSTIDs were 415 ± 28 km and 49 ± 10 min, respectively. The peak to peak amplitude of the MSTIDs varied from −7 to 3%, slightly higher
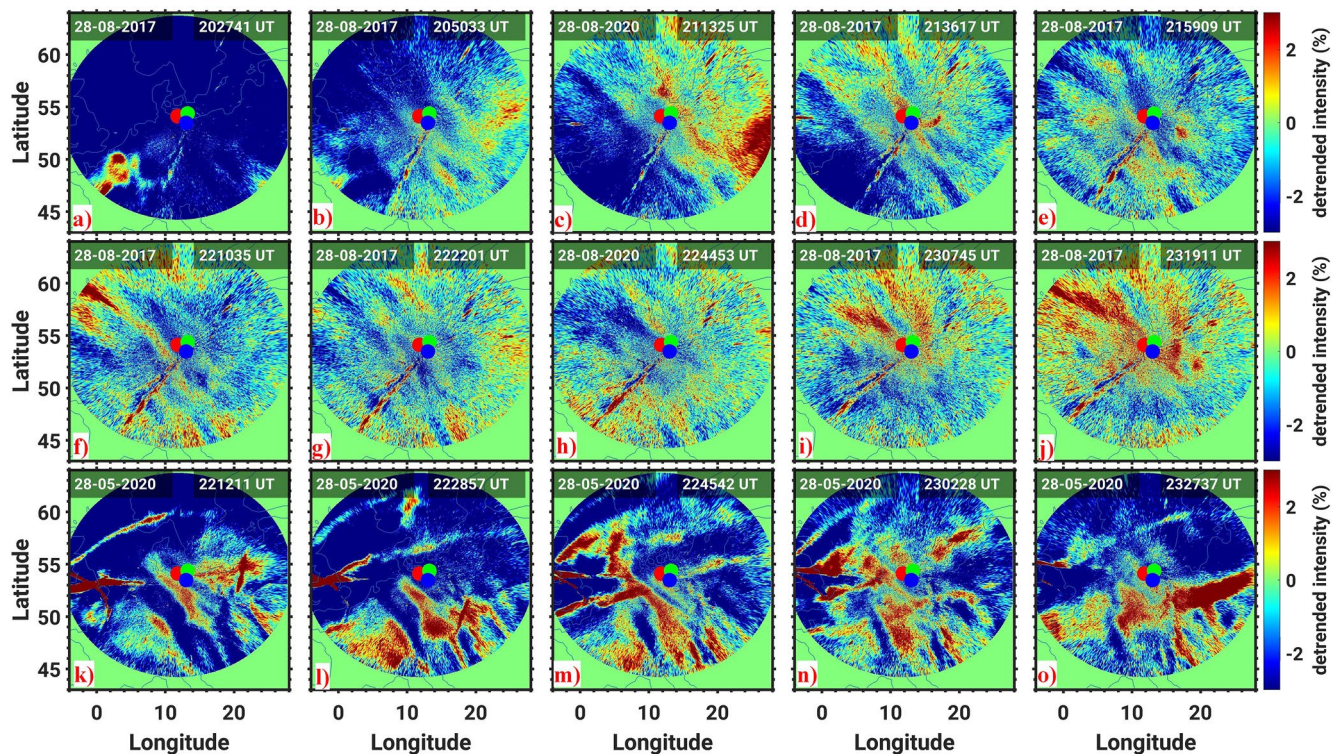
Figure 3. (a–j) Same as Figure 2 but for the summer dates of 28 August 2017 and (k–o) 28 May 2020.

than Events 1 and 2. Two or three tropospheric clouds are also visible in the images as blue bands aligned from the northeast to the southwest. They were confirmed to be clouds through inspection of the background images in 605.0 nm.

Overall, the onsets for Events 1, 2, and 4 occurred over Kühlungsborn, and for Event 3 it was observed ~200–300 km northeast of Kühlungsborn.

3.2. Detrended TEC Perturbations

Two-dimensional detrended total electron content (dTEC) allowed for the visualization of simultaneous electron density perturbations during these four events. Simultaneous dTEC perturbations for equinoctial and local summer nights are shown in Figures 4 and 5, respectively. Movies of dTEC maps for the events are included as Supporting Information (Movies S5–S8).

The dTEC perturbations on 14 March 2020 (Event 1) are shown in Figures 4a–4j where the field of view of the all-sky airglow imager is indicated by a red circle. They began with a northwest to southeast oriented blue band between 60 and 50°N and 2°–16°E in the dTEC maps at 21:40 UT and continued thereafter. This onset is 1 hr after the onset seen in airglow images of the event. The MSTIDs were not visible in the dTEC maps in the earlier hours.

Sample dTEC perturbation images for 23 March 2020 (Event 2) are shown in Figures 4k–4t. A phase front, aligned from the northwest to southeast, propagated southwestward in the dTEC maps between 55 and 45°N and 0°–20°E from 21:35 UT onwards (see Figures 4p–4t). This timing matches observations from the coincident airglow images. The perturbation amplitude was higher for this event when compared with Event 1 (see Movies S5 and S6), though both have a dTEC perturbation amplitude considerably smaller than what is observed for MSTIDs at lower latitudinal locations.

The dTEC perturbation images for Event 3 (28 August 2017) are shown in Figures 5a–5j. A blue band appeared northwest of Kühlungsborn around 19:00 UT, forming in the region between 60 and 55°N and 6°–16°E before
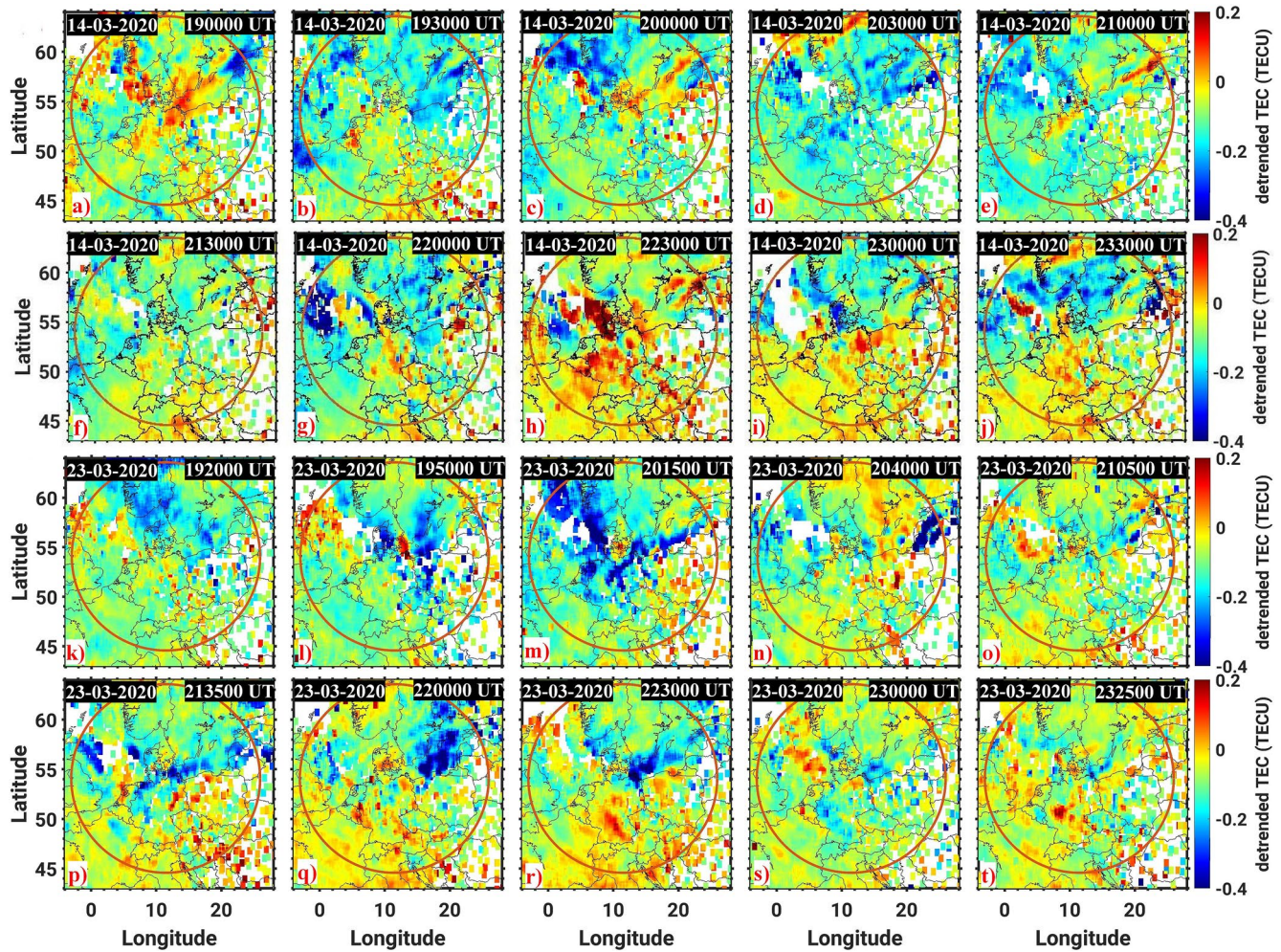
Figure 4. (a–j) Simultaneous detrended total electron content (dTEC) perturbations over northern Europe during the equinoctial dates of 14 March and (k–t) 23 March 2020. The field of view of the airglow imager is highlighted by a red circle. The amplitude of dTEC perturbations increased toward the southern part of the images.

moving toward the southwest. Later on, two prominent blue bands were observed between 20:55 UT and 21:15 UT (see Figure 5c) before soon fading away. These features were consistent with the corresponding airglow observations (see Movie S7). The temporal evolution of the MSTIDs in dTEC perturbations through use of a north-south keogram is detailed in a later.

In Event 4 (28 May 2020), MSTIDs first appeared in the dTEC map around 20:20 UT. Sample dTEC maps are shown in Figures 5k–5t. Two phase fronts, aligned from the northwest to the southeast and colored red and blue, moved southwestward in the dTEC maps between 58 and 45°N and 4°–20°E at around 20:50 UT (see Figure 5l). This indicated that the onset of the MSTIDs occurred sometime before the airglow imager began recording data on this evening. That said, the dTEC maps also show that the generation of the MSTIDs did in fact occur over Kühlungsborn. The amplitude of the TEC perturbation was higher on this night than for Event 3.

Overall, the presence of MSTIDs signatures in the TEC perturbations was consistent with their respective airglow measurements. Furthermore, these observations showed that the amplitudes of the MSTIDs increased toward lower latitudes. Further comparisons between the airglow images, dTEC perturbations and Swarm-A & -C plasma density perturbation can be found in Figure S2 in Supporting Information S1. The dTEC and in situ Swarm-A & -C measurements (at ~300 and ~450 km) showed reasonably good agreement with the ground-based airglow observations (at ~250 km).
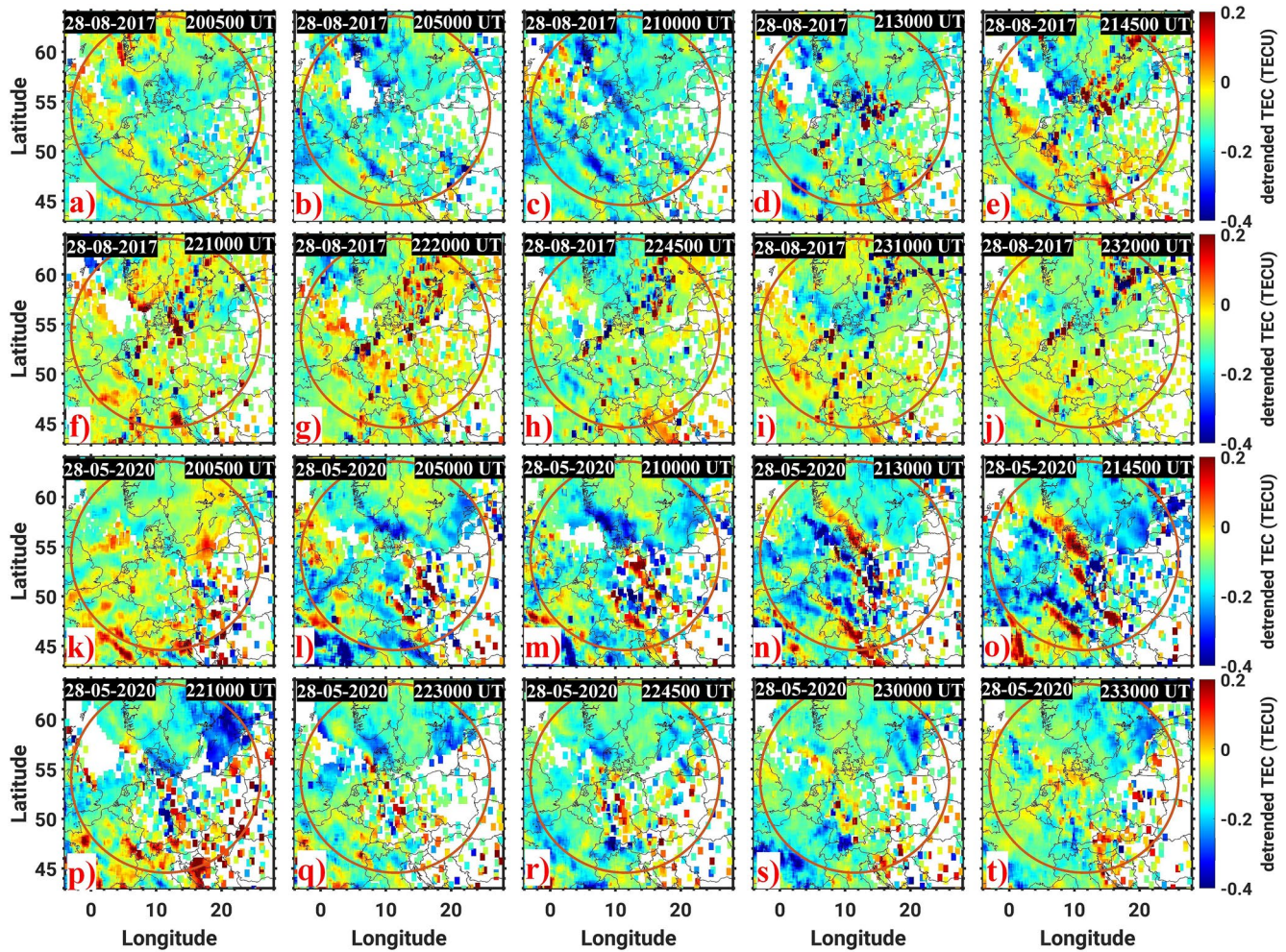
Figure 5. (a–j) Same as Figure 4 but for the summer nights of 28 August 2017 and (k–t) 28 May 2020.

3.3. Ionosonde Observations of E- and F-Region Background Conditions

Simultaneous E- and F-region background conditions, a plausible causative mechanism of nighttime MSTIDs, were investigated using ionosonde measurements from Juliusruh, a site located 120 km northeast of Kühlungsborn. When mapping along magnetic field lines to the altitude of the F-region, the E-region (100 km altitude) is sampled at 54.37°N and 13.2°E, and the F-region at 53.5°N and 13.0°E (250 km altitude) for a horizontal separation of around 100 km. The magnetic inclination and declination angles for both at 100 km are 69.1° and 4.4°, respectively.

The virtual height (h'F) and the critical frequency of the F2 layer (foF2) are parameters that provide the altitude of the bottom of the F-region and the plasma density at the peak of the F-region. Background climatological information was obtained from monthly averages of the hourly median of foF2.

Similarly, characteristics of sporadic-E layer came from measurements of the frequency at which mainly continuous sporadic-E trace is observed (foEs), the frequency up to which the F-layer is blanked out (fbEs) and their difference (foEs-fbEs).

Before detailing the measurements during the four events, we discuss our statistical findings regarding the occurrence of the Es layer during nights with concurrent airglow observations. Out of 226 nights, the Es layer was observed in 118. Of note is that almost every summer night had an Es layer, albeit most having foEs less than 4 MHz. Thirty-six nights had foEs exceed 4 MHz, out of which 17 coincided with observations of MSTIDs in the
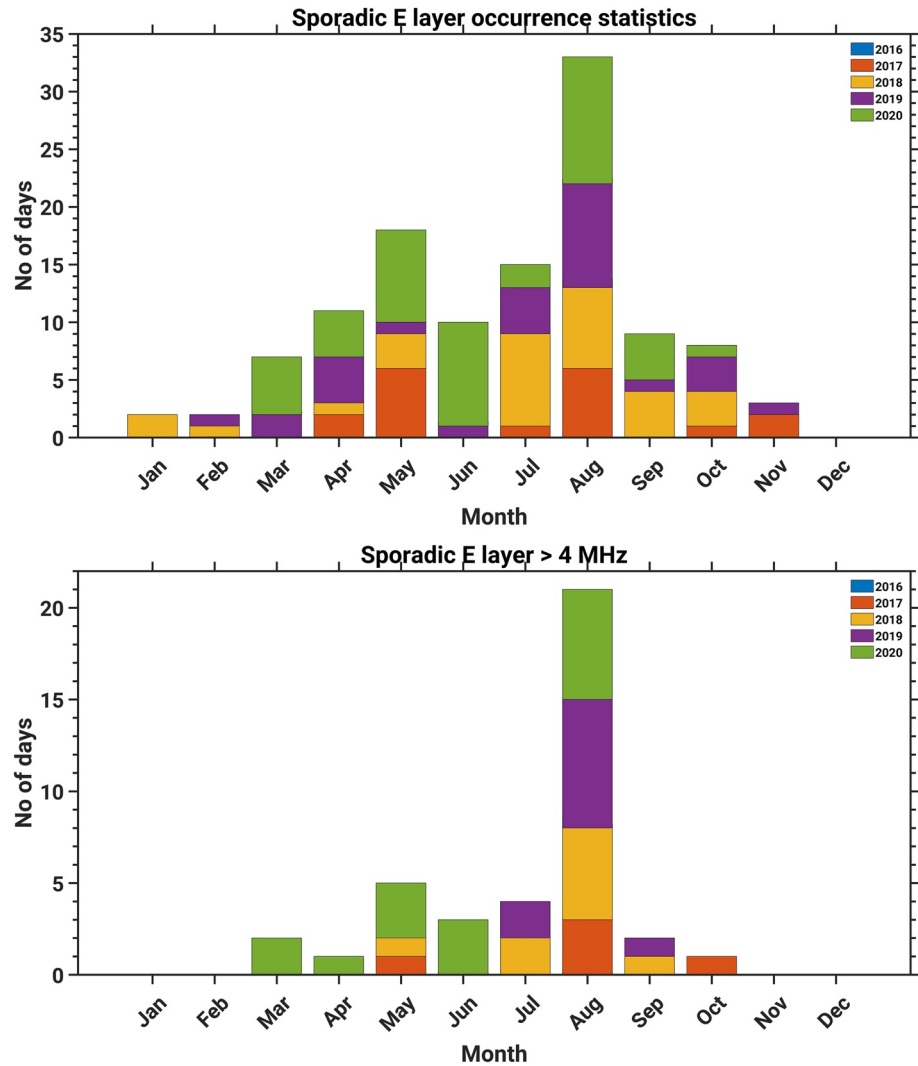
Figure 6. (a) Es layer presence in the ionosonde during the airglow observation nights from December 2016 to December 2020, sorted by month. Figure 6b shows the Es layers with sporadic-E trace is observed ≥4MHz.

airglow images. Monthly Es layer occurrence and Es layer with foEs greater than 4 MHz are shown in Figures 6a and 6b, respectively. These results showed that the onset of MSTIDs over northern Germany requires an Es layer with frequency greater than 4 MHz.

Moving on to the four events, E- and F-region background conditions for nights are shown in Figures 7a–7d and 7e–7h, respectively. With the equinoctial nights, Events 1 and 2, the Es layer was observed around 19:30–20:30 UT and 21:20–24:00 UT, respectively. foEs reached as high as 4 MHz and F-layer is blanked out (fbEs) was very weak. The Es layer occurrence showed a day-to-day variation over these nights. For example, the Es layer was observed for only 1 hour for Event 1 but was observable for more than 3 hr with Event 2. The foF2 (black curve in Figures 7e and 6f) decreased from 19:30 UT to 24:00 UT and was comparable with the monthly (March 2020) average (blue curve in Figures 7e and 7f) for Events 1 and 2. h'F rose by 30–50 km from its earlier position, particularly during the onset of the MSTIDs in the airglow images. Furthermore, a minor (at 20:30–22:00 UT) to moderate (at 22:00–24:00 UT) spread in frequency was observed in Event 1, and a moderate (at 18:00–19:50) to a strong (at 19:50 UT onward) spread-F was observed in Event 2. Thus, on this night the MSTIDs onset and spread-F occurrence times did not coincide.
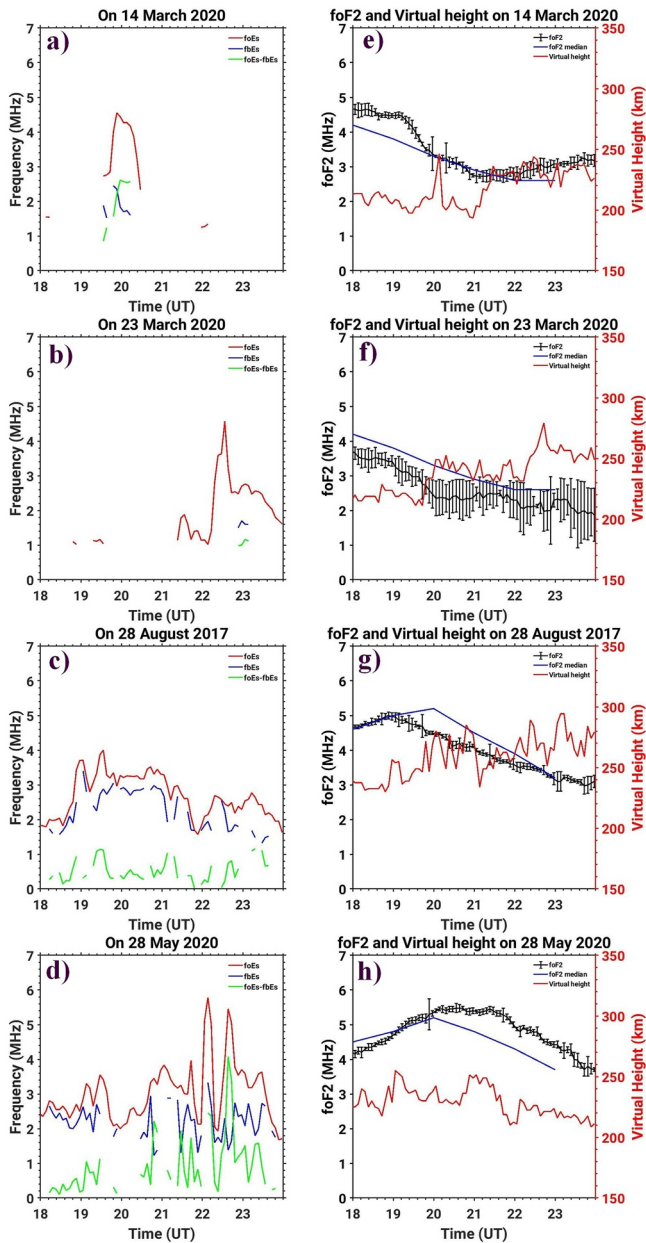
Figure 7. E- and F-region background conditions observed with the Juliusruh ionosonde: (a–d) sporadic-E; (e–h) ionospheric virtual height (h'F), peak plasma frequency (foF2) with standard deviation, and monthly average of foF2 on 14 and 23 2020, 28 August 2017 and 28 May 2020.

For the summer nights (Events 3 and 4), foEs and fbEs were both present in the E-region from 18:00 UT onwards (Figures 7c and 7d). Event 3 had a gradual decrease in foF2 between 19:00 UT and midnight (see Figure 7g). Additionally, h'F ultimately rose by about 25–50 km during the time period MSTIDs observations. Minor to moderate spread-F was observed around ~19:15–19:45 UT, ~21:23 UT and 23:30–24:00 UT. During Event 4, foEs increased after 20:00 UT. foF2 increased from 18:00 UT to 21:00 UT before gradually decreasing, and h'F showed wave-like undulations preceding the onset of the MSTIDs in the airglow images (see Figure 7h). A minor spread-F in the frequency was found around 21:35 UT, strengthening from 23:30 UT onwards. foF2 was slightly higher than the monthly median in both summer events.

An Es layer was observed prior to the onset of MSTIDs in each event. Moreover, the presence of Es layer, an increase of h'F (only in the equinoctial nights, see Figures 7e and 7f), reduction in the foF2, and the onset of MSTIDs in the airglow images all coincided with one another. Event 4 had the largest difference between foEs and fbEs, reaching 4 MHz (see Figure 7d). This difference is a good parameter to estimate the presence of a patchy Es layer in the E-region, which itself is a potential indicator of irregular structures in the Es layer.

We also checked the monthly averages of the hourly median of the foF2 (blue curve in Figures 7e–7h) and found that foF2 decreased after 19:00 UT in March and August. In May, foF2 increased from 18:00 to 21:00 UT before decreasing. One possible cause for this variation between summer and the equinox is the inherent seasonal variation of local sunset in the F-region. Overall, the variations of foF2 were consistent with the monthly median values on these nights.

Ionosonde iso-frequency height-time-intensity (HTI) at various frequencies were used to check the bottom of the F-layer for any undulations (Figures 8a–8d). In Figure 8, red dotted lines denote MSTID onset and disappearance times as identified from the airglow images and dTEC maps. Equinoctial events used a frequency range of 1.6–2.5 MHz to estimate the HTI, and 4–5 MHz for the summer events. Event 1 showed wave undulation in the HTI 40 min after MTSID onset, suggesting the latter caused the former. The opposite was observed with Event 2, with undulations in the HTI preceding the onset of MSTIDs by an hour. That said, oblique ionosonde measurements revealed a traveling ionospheric disturbances (TID) with a 90 min period within Event 2, making this traveling ionospheric disturbances (TID) the likely cause of fluctuations in the HTI as opposed to the MSTID.

The summer events (Events 3 and 4) showed no typical wave oscillations in the HTI. At the very least, this suggested that HTI undulations in the summer have a different source from those during the equinox. The only notable feature in the HTI for the summer events was an enhancement from 19:00 to 21:00 UT for Event 3. This seemingly contradicted observations from the other events. The only other event to have wave undulation in the HTI maps prior to MSTID onset was Event 2, where wave undulations were observed from 19:30 UT onwards. However, the onset of the MSTIDs was noted only around 21:20 UT, a time that coincided with the Es layer occurrence. Therefore, we believe that the gravity waves could not be a source for the generation of the MSTIDs on these nights.

Another important parameter to observe is the altitude of the Es layer, and any effect it may have on the generation of MSTIDs. As such, the virtual height of the Es layer (h'Es) is shown in Figure 9. The error in h'Es (lowest height of the trace) was ±2.5 km. With Event 1, the Es layer appeared around 97 km at 19:30 UT and ascended to
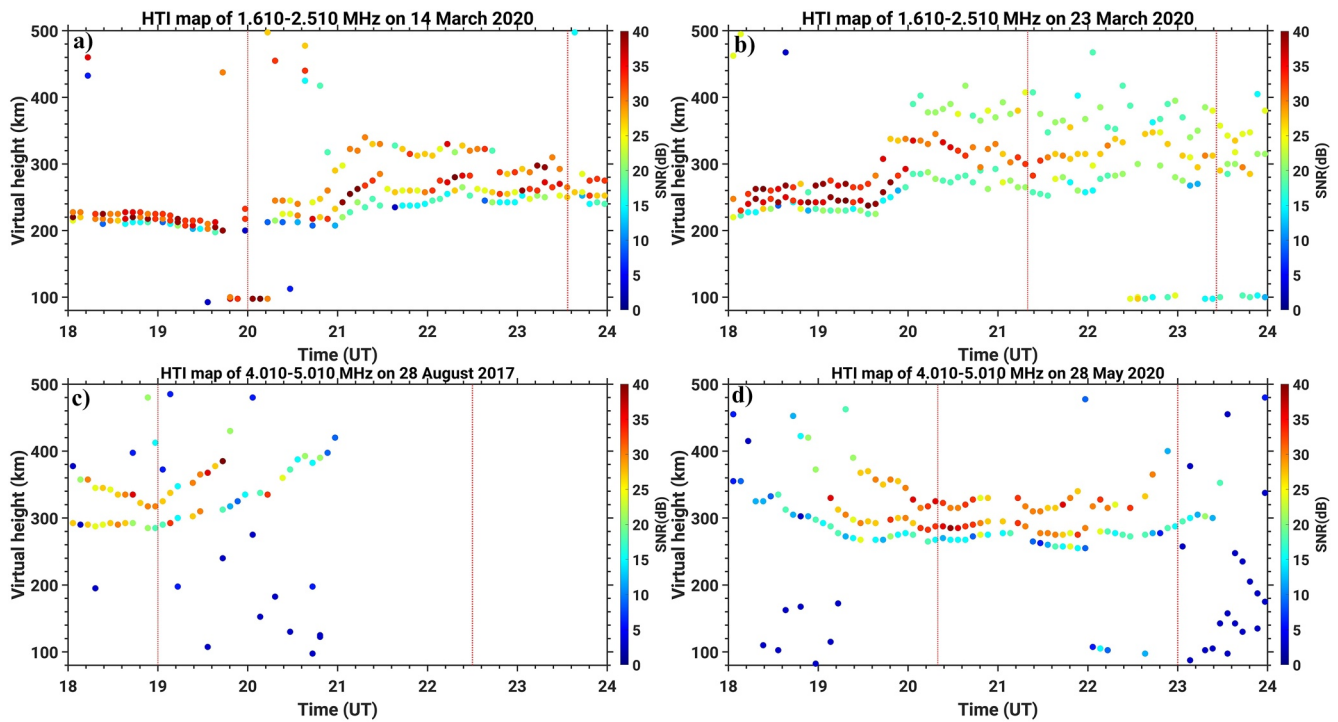
Figure 8. Ionosonde iso-frequency height time intensity (HTI) variations on 14 and 23 March 2020, 28 August 2017 and 28 May 2020. Onset and disappearance time of medium-scale traveling ionospheric disturbances as seen in airglow images is highlighted by dotted red lines.

102 km around 20:00 UT. This window of time encapsulates the onset of MSTIDs as seen in the airglow images. The Es layer appeared around 21:20 UT for Event 2, during which h'Es started at 104 km before gradually descending at a rate of approximately 1.4 m/s. This also coincided with the time of MSTID onset for the event.

Both summer events had an Es layer appearing at a higher altitude from 18:00 UT onwards. Event 3 had the Es layer appear at 114 km and h'Es descend at approximately 1.6 m/s, while Event 4 had an altitude of 112 km and descent of ~2.7 m/s. These rates of descent suggested that the semidiurnal tides associated with wind shear nodes may cause descent in the Es layer (Haldoupis et al., 2006). At the time of MSTID onset, h'Es was around 112 km for Event 3 and 102 km for Event 4. In sum, the onset of MSTIDs was observed when the Es layer is present at an altitude range of 100–110 km, particularly around 105 km. This altitude range is consistent with an earlier model study by Cosgrove (2007), in which he considered the altitude of the Es layer as 105 km in simulations. This is the same altitude where the Hall and Cowling conductivity peaks. Thus, our results provide supporting observational evidence that the altitude of the Es layer has an essential role in the onset of MSTIDs by way of the Es layer and F-region coupling process.

3.4. Coincidence of Es Layer and MSTIDs Occurrence

A north-south (NS) keogram was constructed using a strip (9°–11°E longitudinal average) of airglow and dTEC maps for each time with latitudinal variation. Keograms can provide detailed information about the temporal evolution of MSTIDs. To provide a concise preview of the MSTIDs and Es layer characteristics, the dTEC and airglow north-south (NS) keograms are plotted together with Es layer in Figure 10. Onset and disappearance times of the MSTIDs are marked by red dotted lines. In Events 1 and 2 (14 and 23 March 2020), two southward propagating phase fronts were visible in the airglow residual intensity keogram, originating from around 55°N (see Figures 10b and 10e). However, in the dTEC keogram, the phase fronts were feeble (see Figures 10a and 10d). Perhaps more importantly, the onset of MSTIDs coincided with the Es layer occurrence and the time when the magnitude of foEs reached more than 4 MHz (see Figures 10c and 10f).
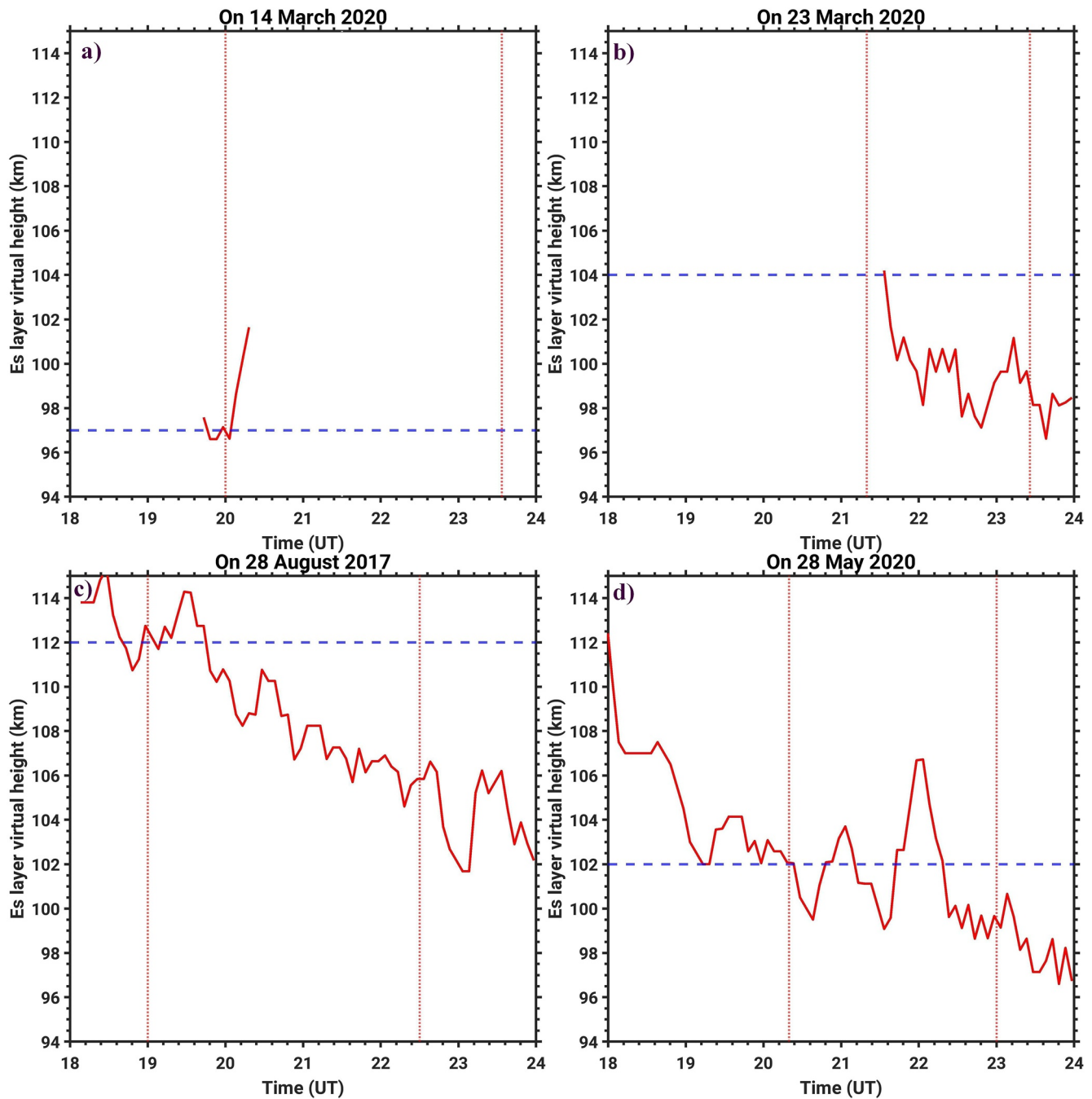
Figure 9. (a–b) Virtual height of the Es layer variations on 14 and 23 March 2020, 28 August 2017 and (c–d) 28 May 2020. medium-scale traveling ionospheric disturbances onset times (vertical line) in the airglow images and the corresponding Es layer altitudes (horizontal line) are highlighted by blue dotted lines.

In Events 3 and 4 (28 August 2017 and 28 May 2020), two southward moving blue bands were observed in the dTEC keogram (see Figures 10g and 10j) between 60 and 50°N at around 19:00 UT and 20:24 UT, respectively. Airglow residual intensity keograms showed similar kinds of phase fronts as shown in Figures 10h and 10k. Onset of the MSTIDs was identified using the dTEC keogram, since the airglow observations began later in the evening. The Es layer with foEs ≥ 4 MHz is also observed on these nights (see Figures 10i and 10l). With Event 4, the amplitude of the MSTIDs increased alongside the magnitude of foEs. Amongst all four events, the amplitude of the MSTIDs was smallest with Event 3. Onset and disappearance time of the MSTIDs and Es layers are given in Table 2.
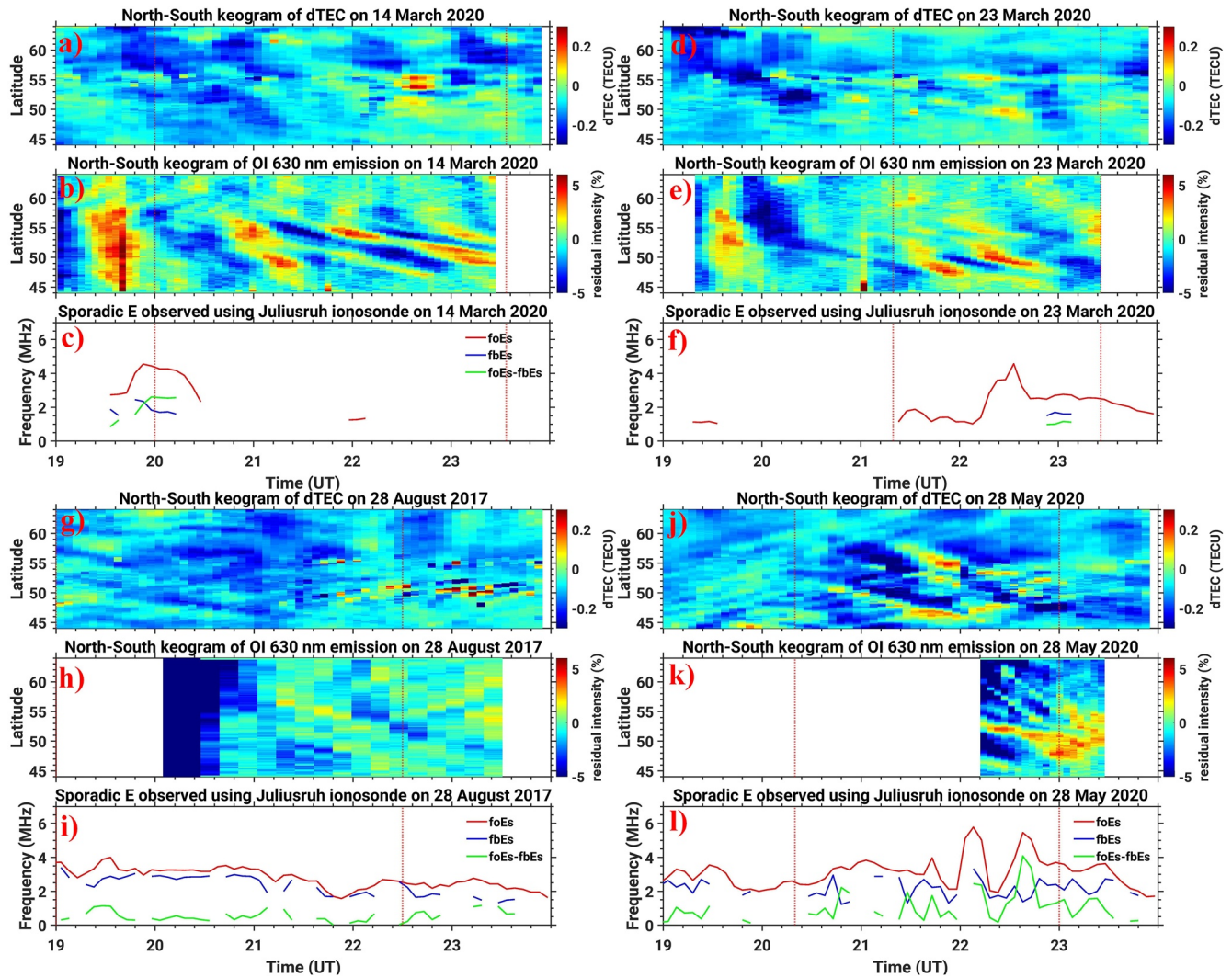
Figure 10. (a–c) Comparison of temporal evolution of the medium-scale traveling ionospheric disturbances (MSTIDs) in the detrended total electron content and airglow images as well as Es layer in the ionosonde observations for March 14 and (d–f) 23, 2020, 28 August 2017 (g–i) and 28 May 2020 (j–l). Onset and disappearance times of the MSTIDs are marked by red dotted lines.

4. Discussion

MSTIDs are typical phenomena that occur in the mid-latitude ionosphere. Despite this, the causative mechanism for their onset during nighttime MSTIDs is still an unanswered question for the ionospheric community to ponder. Over the last three decades, several investigations have reported on the various characteristics of MSTIDs. In particular, advancements in the 2-dimensional optical airglow imaging was used to explore the struc-

Table 2
Onset and Disappearance Time of the Es Layer, MSTIDs and Spread-F Observed in the Airglow Images, dTEC and Ionosonde Observations

Date	Es layer		MSTIDs		Spread-F (status)	
	Onset (UT)	Disappearance (UT)	Onset (UT)	Disappearance (UT)	Onset (UT)	Disappearance (UT)
14.03.2020	19:30	20:30	20:03	23:34	19:30	24:00 (minor)
23.03.2020	21:24	24:00	21:20	23:24	18:00	24:00 (minor to strong)
28.08.2017	18:00	24:00	19:00	22:30	21:40	24:00 (minor to moderate, frequent interval)
28.05.2020	18:00	24:00	20:20	23:00	19:00	24:00 (minor to moderate, frequent interval)

ture and propagation characteristics of the nighttime MSTIDs. Perkins instability was initially proposed to explain the phase front alignment and generation of the nighttime MSTIDs. However, the growth rate of the Perkins instability is very small. This problem was remedied when further developments in model simulations and rocket experiments suggested that the growth rate of the Perkins instability was enhanced by an order of magnitude in the presence of Es layer instabilities in the E-region (Cosgrove, 2013 and reference therein). Therefore, coupling between the E- and F-region instabilities is a potential source for the generation of nighttime MSTIDs.

The present observations show that the occurrence of southwest moving MSTIDs is infrequent over Kühlungsborn as compared to the other mid-latitude sites. In order to know if geomagnetic disturbances on these nights were present, we investigated the *Kp* index for the 2–3 hr prior (i.e., at 18:00 UT) to MSTIDs onset. *Kp* was ≤1 for three events, namely, Events 1, 3 and 4. *Kp* index for Event 2 was 3⁺. These suggest that geomagnetic disturbances were not a source for the onset of these MSTIDs.

Using a suite of observations from the E- and F-region, the present study now focuses primarily on two questions: (a) How high in latitude do MSTIDs extend? (b) What is the role of the ionospheric background conditions and Es layer instabilities in the generation of MSTIDs?

4.1. Onset Location of the MSTIDs: Latitude Dependency

The unwarped field of view of the Kühlungsborn all-sky imager covers the area from about −2 to 28°E and 46–63°N (see Figures 2 and 3) when mapped to 250 km and using 80° zenith angle. With all four events, the onset of the MSTIDs was observed below 60°N. Simultaneous GNSS 2-dimensional detrended TEC also showed the presence of southwest moving MSTIDs, albeit with a weak, particularly during equinoctial events. These amplitudes were smaller than those observed in mid-latitude MSTIDs. For example, Huang et al. (2016), using 3 years of airglow and GNSS-TEC observations, reported that the amplitude of the nighttime MSTIDs showed a year to year variation of ∼5–10% at a mid-latitude station over China. In the present cases, MSTID amplitudes ranged from 2% to 6%. Moreover, we observed that the amplitude increased toward the equator (see keograms in Figure 10).

The next factor to consider is the role of dip angle (I) on the latitudinal variation of nighttime MSTIDs. The study by Otsuka et al. (2013) showed that the nighttime MSTIDs had almost 50% variation in occurrence rate between $I = 63.5°$ and 74.2° over northern Europe. Their investigation showed that the amplitude of nighttime dTEC perturbations associated with the MSTIDs varies with dip angle, that is, the amplitude decreased as dip angle increased. They also showed that the nighttime MSTIDs occurrence was low above 55°N in the European sector. In the present study, the field of view of the imager covers the dip angles between 61.87° and 74.4°, stretching from the bottom to the top of the image (at zenith, dip angle is 68.6°). As such, our results are consistent with the findings from Otsuka et al. (2013). Additionally, plasma motion in the F-region due to ExB drift is nearly horizontal at large dip angles, resulting in a small vertical modulation of the bottom side of F-region. This is another effect that could contribute to the reduced occurrence rate and amplitude of MSTIDs over Kühlungsborn.

A study by Yokoyama and Hysell (2010) used a model simulation to argue that the growth rate of the Es layer and Perkins instabilities showed latitudinal dependency because these instability growth rates were directly proportional to the ratio of the field line integrated Hall and Pedersen conductivity and the cosine of the dip angle (Yokoyama & Hysell, 2010). More specifically, the field line integrated Hall and Pedersen conductivity ratio is larger at lower latitudes due to more efficient wind shear convergence of an Es layer. As a result, the growth rate of these instabilities decreases toward high latitudes. Thus, we can assume that the high dip angle and low field line integrated conductivity ratio were at least partially responsible for the low occurrence of nighttime MSTIDs at this high mid-latitude site.

4.2. E and F Region Coupling

As previously stated, the Perkins instability alone cannot explain the growth rate of nighttime MSTIDs (e.g., Garcia et al., 2000; Miller et al., 1997; Shiokawa, Ihara, et al., 2003; Shiokawa, Otsuka, et al., 2003; Sivakandan et al., 2020). Yokoyama et al. (2009) used a simulation to show that E- and F-region coupling through Es layer instability and Perkins instability plays an important role in the generation of nighttime MSTIDs. Previous

theoretical studies had highlighted the relevance of E- and F-region coupling in the generation of MSTIDs, which is why this study has focused on the E- and F-region coupling process.

The critical point here is that all four events had an onset of MSTIDs in the presence of an Es layer with foEs around 4 MHz. This is similar to the findings from Narayanan et al. (2018), where MSTIDs occurred whe foEs exceeded 6 MHz over the mid-latitudes of the Japanese sectors in the north and Australian in the south. When taken together, Narayanan et al. (2018) and the present investigation suggest that the presence of an Es layer is required for the onset of MSTIDs.

The four events studied here showed that in each case, the source of the onset of the MSTIDs was present in the E-region of the same hemisphere as it was observed. Put plainly, the events were observed in the northern hemisphere and their sources were also in the E-region of the northern hemisphere. This finding is consistent with a recent climatological study by Lee et al. (2021), in which the onset of nighttime MSTIDs was shown to be linked to the Es layer in the local hemisphere during the equinox and summer conditions.

The next factor to consider is that of the altitude of the Es layer during the onset of MSTIDs. Hall conductivity, which peaks around 105 km, is proportional to the growth rate of Es layer instability (Cosgrove & Tsunoda, 2002). Furthermore, the strength of the Hall polarization electric field—obtained by mapping to the F-region via magnetic field lines—is determined by the ratio of Hall conductance to the sum of the E- and F-region Pedersen conductance (Tsunoda & Cosgrove, 2001). All this suggests that the altitude of the Es layer plays an important role in the onset of MSTIDs, and indeed the altitudes at MSTID onset in the events of this study congregated between 102 and 110 km, a range encompassing the peak of Hall conductivity.

As mentioned in the introduction, the ratio of the field line integrated Hall conductivity of the Es layer to the field line integrated Pedersen conductivity of the F-region has an important role in controlling the influence of the E-region polarization electric field on the F-region. Earlier model simulations suggested that Es-instabilities with large polarization electric fields (>10 mV/m) could effectively map onto the F-region when the F-region conductance is low (Cosgrove et al., 2004). Moreover, the Hall and Pedersen conductance variations are sensitive to the altitude modulation of the Es layer and F-layer and are important to the density perturbation (Yokoyama & Hysell, 2010).

Studies using model simulations showed the direction of the wind flow and shear in the neutral wind as predominant sources for the generation of Es layers in the mid-latitude ionosphere (Yokoyama et al., 2009; Yokoyama & Hysell, 2010). Thus, we believe that wind shear could cause the formation of the Es layer on these nights. It is common to observe the Es layer during the summer (Yu et al., 2021). Despite this, we observed two instances in which the Es layer not only appeared during the equinox but also coincided with the onset of MSTIDs, opening up entirely new questions: (a) will the presence of an Es layer during the equinox always trigger the onset of MSTIDs? (b) What causes the large shear in the horizontal winds during the equinox and how much does it contribute to the formation of Es layer? These questions will be addressed in future studies.

5. Summary and Conclusion

Occurrence characteristics of nighttime MSTIDs over the high mid-latitude transition region of Kühlungsborn, Germany were studied using simultaneous measurements from OI 630 nm airglow, GNSS dTEC, and ionosonde data. Airglow imaging observations showed that out of 226 nights with clear skies for more than 3 hr, only 18 had MSTIDs. All but one of the 18 nights had an Es layer with foEs greater than 4 MHz.

This study examined four MSTID events: two during vernal equinox and two during local summer. Aspects of each event, such as time of onset, direction of propagation and measurements of the E- and F-regions were carefully considered. The wavelength and phase velocity of these MSTIDs varied from 300 to 450 km and 60 to 150 m/s, respectively. The important findings are summarized below.

1. Onset of all four events, as viewed by the airglow imager, was observed between 15 and 20°E and 55–45°N. Each had structures propagate toward the southwest. The presence of southwestwardly propagating MSTIDs was confirmed by coincident GNSS 2D detrended-TEC maps.

2. The amplitude of the MSTIDs' phase fronts were enhanced upon reaching the southwestern region of the airglow images. Overall, the amplitudes of these MSTIDs are significantly weaker than those of mid-latitude MSTIDs.

3. All nights had an observable Es layer and a varying foEs. At some point during each night, foEs exceeded 4 MHz. The fact that the onset of the MSTIDs occurred in the presence of Es layer in each case supports the theory that onset is related to a coupled Es layer and F-region instabilities. During the events, the Es layer existed at an altitude of 102–110 km, coinciding with the peak of Hall conductivity.

The observed nighttime MSTIDs could be caused by the coupling process between the Perkins and Es layer instabilities. From the observational results described above, we reach the following conclusions:

1. The low occurrence rate and small amplitude of nighttime MSTID over Kühlungsborn may be attributable to the dip angle dependence of the Es layer instability. The growth rate of the Es layer instability is proportional to cosine of the dip angle, represented by a decrease in occurrence rate and amplitude of MSTIDs at higher magnetic latitudes. At large dip angles, the plasma motion in the F-region due to ExB drift is nearly horizontal, and thus vertical modulation of the bottom side of F-region becomes small. This effect could also contribute to the reduced occurrence rate and amplitude of MSTIDs.

2. An Es layer with foEs $\geq$ 4 MHz is a potential seeding factor for the onset of MSTIDs over Kühlungsborn. Another important factor to consider is the altitude of Es layer. Observations of the Es layer in each event coincided with the peak of the Hall conductivity, suggesting that when the Es layer exists around an altitude where the Hall conductivity is large, MSTIDs could be amplified through the Es layer instability.

Data Availability Statement

The airglow imager data is available at http://sirius.bu.edu/data/. The ionosonde data is available through the following link https://lgdc.uml.edu/common/DIDBYearListForStation?ursiCode=JR055. Data from the Swarm mission are provided at http://swarm-diss.eo.esa.int.

References

Behnke, R. (1979). F layer height bands in the nocturnal ionosphere over Arecibo. *Journal of Geophysical Research*, *84*(A3), 974–978. https://doi.org/10.1029/JA084iA03p00974

Belehaki, A., Tsagouri, I., Altadill, D., Blanch, E., Borries, C., Buresova, D., et al. (2020). An overview of methodologies for real-time detection, characterisation and tracking of traveling ionospheric disturbances developed in the TechTIDE project. *Journal of Space Weather and Space Climate*, *10*, 42. https://doi.org/10.1051/swsc/2020043

Bowman, G. G. (1990). A review of some recent work on mid-latitude spread-F occurrence as detected by ionosondes. *Journal of Geomagnetism and Geoelectricity*, *42*(2), 109–138. https://doi.org/10.5636/jgg.42.109

Bowman, G. G., & Monro, P. E. (1988). Mid-latitude range spread and travelling ionospheric disturbances. *Journal of Atmospheric and Terrestrial Physics*, *50*(3), 215–223. https://doi.org/10.1016/0021-9169(88)90070-0

Cosgrove, R. (2013). Mechanisms for E-F coupling and their manifestation. *Journal of Atmospheric and Solar-Terrestrial Physics*, *103*, 56–65. https://doi.org/10.1016/j.jastp.2013.03.011

Cosgrove, R. B. (2007). Generation of mesoscale F layer structure and electric fields by the combined Perkins and Es layer instabilities, in simulations. *Annales Geophysicae*, *25*(7), 1579–1601. https://doi.org/10.5194/angeo-25-1579-2007

Cosgrove, R. B., & Tsunoda, R. T. (2002). A direction-dependent instability of sporadic-*E* layers in the nighttime midlatitude ionosphere. *Geophysical Research Letters*, *29*(18), 1864. https://doi.org/10.1029/2002GL014669

Cosgrove, R. B., Tsunoda, R. T., Fukao, S., & Yamamoto, M. (2004). Coupling of the Perkins instability and the sporadic E layer instability derived from physical arguments. *Journal of Geophysical Research*, *109*(A6), 1–11. https://doi.org/10.1029/2003JA010295

Duly, T. M., Chapagain, N. P., & Makela, J. J. (2013). Climatology of nighttime medium-scale traveling ionospheric disturbances (MSTIDs) in the Central Pacific and South American sectors. *Annales Geophysicae*, *31*(12), 2229–2237. https://doi.org/10.5194/angeo-31-2229-2013

Garcia, F. J., Kelley, M. C., Makela, J. J., & Huang, C.-S. (2000). Airglow observations of mesoscale low-velocity traveling ionospheric disturbances at midlatitudes. *Journal of Geophysical Research*, *105*(A8), 18407–18415. https://doi.org/10.1029/1999JA000305

Haldoupis, C., Kelley, M. C., Hussey, G. C., & Shalimov, S. (2003). Role of unstable sporadic-E layers in the generation of midlatitude spread F. *Journal of Geophysical Research*, *108*(A12), 1–8. https://doi.org/10.1029/2003JA009956

Haldoupis, C., Meek, C., Christakis, N., Pancheva, D., & Bourdillon, A. (2006). Ionogram height-time-intensity observations of descending sporadic E layers at mid-latitude. *Journal of Atmospheric and Solar-Terrestrial Physics*, *68*(3–5), 539–557. https://doi.org/10.1016/j.jastp.2005.03.020

Huang, F., Dou, X., Lei, J., Lin, J., Ding, F., & Zhong, J. (2016). Statistical analysis of nighttime medium-scale traveling ionospheric disturbances using airglow images and GPS observations over central China. *Journal of Geophysical Research: Space Physics*, *121*(9), 8887–8899. https://doi.org/10.1002/2016JA022760

Kotake, N., Otsuka, Y., Ogawa, T., Tsugawa, T., & Saito, A. (2007). Statistical study of medium-scale traveling ionospheric disturbances observed with the GPS networks in Southern California. *Earth Planets and Space*, *59*(2), 95–102. https://doi.org/10.1186/BF03352681

Lee, C. C., Liou, Y. A., Otsuka, Y., Chu, F. D., Yeh, T. K., Hoshinoo, K., & Matunaga, K. (2008). Nighttime medium-scale traveling ionospheric disturbances detected by network GPS receivers in Taiwan. *Journal of Geophysical Research*, *113*(A12), A12316. https://doi.org/10.1029/2008JA013250

Lee, W. K., Kil, H., & Paxton, L. J. (2021). Global distribution of nighttime MSTIDs and its association with E region irregularities seen by CHAMP satellite. *Journal of Geophysical Research: Space Physics*, *126*(5), e2020JA028836. https://doi.org/10.1029/2020JA028836

Martinis, C., Baumgardner, J., Mendillo, M., Wroten, J., MacDonald, T., Kosch, M., et al. (2019). First conjugate observations of medium scale travelling ionospheric disturbances (MSTIDs) in the Europe-Africa longitude sector. *Journal of Geophysical Research: Space Physics*, *124*(3), 2213–2222. https://doi.org/10.1029/2018JA026018

Martinis, C., Baumgardner, J., Wroten, J., & Mendillo, M. (2010). Seasonal dependence of MSTIDs obtained from 630.0 nm airglow imaging at Arecibo. *Geophysical Research Letters*, *37*(11), 2000–2004. https://doi.org/10.1029/2010GL043569

Martinis, C., Baumgardner, J., Wroten, J., & Mendillo, M. (2011). All-sky imaging observations of conjugate medium-scale traveling ionospheric disturbances in the American sector. *Journal of Geophysical Research*, *116*(A5), A05326. https://doi.org/10.1029/2010JA016264

Martinis, C., Baumgardner, J., Wroten, J., & Mendillo, M. (2018). All-sky-imaging capabilities for ionospheric space weather research using geomagnetic conjugate point observing sites. *Advances in Space Research*, *61*(7), 1636–1651. https://doi.org/10.1016/j.asr.2017.07.021

Miller, C. A., Swartz, W. E., Kelley, M. C., Mendillo, M., Nottingham, D., Scali, J., & Reinisch, B. (1997). Electrodynamics of midlatitude spread F: 1. Observations of unstable, gravity wave-induced ionospheric electric fields at tropical latitudes. *Journal of Geophysical Research*, *102*(A6), 11521–11532. https://doi.org/10.1029/96JA03839

Narayanan, V. L., Patra, A. K., Gurubaran, S., Pavan Chaitanya, P., & Emperumal, K. (2019). Coincident airglow, VHF Radar, and ionosonde observations of electrified medium-Scale traveling ionospheric disturbances in the equatorial latitudes. *Geophysical Research Letters*, *46*(13), 7173–7181. https://doi.org/10.1029/2019GL083266

Narayanan, V. L., Shiokawa, K., Otsuka, Y., & Neudegg, D. (2018). On the Role of thermospheric winds and sporadic E layers in the formation and evolution of electrified MSTIDs in geomagnetic conjugate regions. *Journal of Geophysical Research: Space Physics*, *123*(8), 6957–6980. https://doi.org/10.1029/2018JA025261

Narayanan, V. L., Shiokawa, K., Otsuka, Y., & Saito, S. (2014). Airglow observations of nighttime medium-scale traveling ionospheric disturbances from Yonaguni: Statistical characteristics and low-latitude limit. *Journal of Geophysical Research: Space Physics*, *119*(11), 9268–9282. https://doi.org/10.1002/2014JA020368

Otsuka, Y., Shinbori, A., Tsugawa, T., & Nishioka, M. (2021). Solar activity dependence of medium-scale traveling ionospheric disturbances using GPS receivers in Japan. *Earth Planets and Space*, *73*(1), 22. https://doi.org/10.1186/s40623-020-01353-5

Otsuka, Y., Shiokawa, K., Ogawa, T., & Wilkinson, P. (2004). Geomagnetic conjugate observations of medium-scale traveling ionospheric disturbances at midlatitude using all-sky airglow imagers. *Geophysical Research Letters*, *31*(15), L15803. https://doi.org/10.1029/2004gl020262

Otsuka, Y., Suzuki, K., Nakagawa, S., Nishioka, M., Shiokawa, K., & Tsugawa, T. (2013). GPS observations of medium-scale traveling ionospheric disturbances over Europe. *Annales Geophysicae*, *31*(2), 163–172. https://doi.org/10.5194/angeo-31-163-2013

Otsuka, Y., Tani, T., Tsugawa, T., Ogawa, T., & Saito, A. (2008). Statistical study of relationship between medium-scale traveling ionospheric disturbance and sporadic E layer activities in summer night over Japan. *Journal of Atmospheric and Solar-Terrestrial Physics*, *70*(17), 2196–2202. https://doi.org/10.1016/j.jastp.2008.07.008

Perkins, F. (1973). Spread F and ionospheric currents. *Journal of Geophysical Research*, *78*(1), 218–226. https://doi.org/10.1029/JA078i001p00218

Reinisch, B. W., & Galkin, I. A. (2011). Global ionospheric radio observatory (GIRO). *Earth Planets and Space*, *63*(4), 377–381. https://doi.org/10.5047/eps.2011.03.001

Reinisch, B. W., Galkin, I. A., Khmyrov, G. M., Kozlov, A. V., Lisysyan, I. A., Bibl, K., et al. (2008). Advancing Digisonde technology: The DPS-4D. *AIP Conference Proceedings*, *974*, 127–143. https://doi.org/10.1063/1.2885022

Saito, S., Yamamoto, M., Hashiguchi, H., Maegawa, A., & Saito, A. (2007). Observational evidence of coupling between quasi-periodic echoes and medium scale traveling ionospheric disturbances. *Annales Geophysicae*, *25*(10), 2185–2194. https://doi.org/10.5194/angeo-25-2185-2007

Shiokawa, K., Ihara, C., Otsuka, Y., & Ogawa, T. (2003). Statistical study of nighttime medium-scale traveling ionospheric disturbances using midlatitude airglow images. *Journal of Geophysical Research*, *108*(A1), 1–7. https://doi.org/10.1029/2002JA009491

Shiokawa, K., Mori, M., Otsuka, Y., Oyama, S., Nozawa, S., Suzuki, S., & Connors, M. (2013). Observation of nighttime medium-scale travelling ionospheric disturbances by two 630-nm airglow imagers near the auroral zone. *Journal of Atmospheric and Solar-Terrestrial Physics*, *103*, 184–194. https://doi.org/10.1016/j.jastp.2013.03.024

Shiokawa, K., Otsuka, Y., Ejiri, M. K., Sahai, Y., Kadota, T., Ihara, C., et al. (2002). Imaging observations of the equatorward limit of midlatitude traveling ionospheric disturbances. *Earth Planets and Space*, *54*(1), 57–62. https://doi.org/10.1186/BF03352421

Shiokawa, K., Otsuka, Y., Ihara, C., Ogawa, T., & Rich, F. J. (2003). Ground and satellite observations of nighttime medium-scale traveling ionospheric disturbance at midlatitude. *Journal of Geophysical Research*, *108*(A4), 1–13. https://doi.org/10.1029/2002JA009639

Shiokawa, K., Otsuka, Y., Tsugawa, T., Ogawa, T., Saito, A., Ohshima, K., et al. (2005). Geomagnetic conjugate observation of nighttime medium-scale and large-scale traveling ionospheric disturbances: FRONT3 campaign. *Journal of Geophysical Research*, *110*(A5), A05303. https://doi.org/10.1029/2004JA010845

Sivakandan, M., Chakrabarty, D., Ramkumar, T. K., Guharay, A., Taori, A., & Parihar, N. (2019). Evidence for deep ingression of the midlatitude MSTID into as low as ~3.5° magnetic latitude. *Journal of Geophysical Research: Space Physics*, *124*(1), 749–764. https://doi.org/10.1029/2018JA026103

Sivakandan, M., Mondal, S., Sarkhel, S., Chakrabarty, D., Sunil Krishna, M. V., Chaitanya, P. P., et al. (2020). Mid-latitude spread-F structures over the geomagnetic low-mid latitude transition region: An observational evidence. *Journal of Geophysical Research: Space Physics*, *125*(5), e2019JA027531. https://doi.org/10.1029/2019JA027531

Takahashi, H., Wrasse, C. M., Figueiredo, C. A. O. B., Barros, D., Abdu, M. A., Otsuka, Y., & Shiokawa, K. (2018). Equatorial plasma bubble seeding by MSTIDs in the ionosphere. *Progress in Earth and Planetary Science*, *5*(1), 32. https://doi.org/10.1186/s40645-018-0189-2

Terra, P., Vargas, F., Brum, C. G. M., & Miller, E. S. (2020). Geomagnetic and solar dependency of MSTIDs occurrence rate: A climatology based on airglow observations from the arecibo observatory ROF. *Journal of Geophysical Research: Space Physics*, *125*(7), e2019JA027770. https://doi.org/10.1029/2019JA027770

Tsunoda, R. T., & Cosgrove, R. B. (2001). Coupled electrodynamics in the nighttime midlatitude ionosphere. *Geophysical Research Letters*, *28*(22), 4171–4174. https://doi.org/10.1029/2001gl013245

Yokoyama, T. (2014). Hemisphere-coupled modeling of nighttime medium-scale traveling ionospheric disturbances. *Advances in Space Research*, *54*(3), 481–488. https://doi.org/10.1016/j.asr.2013.07.048

Yokoyama, T., & Hysell, D. L. (2010). A new midlatitude ionosphere electrodynamics coupling model (MIECO): Latitudinal dependence and propagation of medium-scale traveling ionospheric disturbances. *Geophysical Research Letters*, *37*(8), 1–5. https://doi.org/10.1029/2010GL042598

Yokoyama, T., Hysell, D. L., Otsuka, Y., & Yamamoto, M. (2009). Three-dimensional simulation of the coupled Perkins and es-layer instabilities in the nighttime midlatitude ionosphere. *Journal of Geophysical Research*, *114*(3), 1–16. https://doi.org/10.1029/2008JA013789

Yu, B., Xue, X., Scott, C. J., Wu, J., Yue, X., Feng, W., et al. (2021). Interhemispheric transport of metallic ions within ionospheric sporadic E layers by the lower thermospheric meridional circulation. *Atmospheric Chemistry and Physics*, *21*(5), 4219–4230. https://doi.org/10.5194/acp-21-4219-2021